PNAS
www.pnas.org

Supplementary Information for

Disruption of the circadian clock component BMAL1 elicits an endocrine adaption impacting on insulin sensitivity and liver disease

Céline Jouffe, Benjamin D. Weger, Eva Martin, Florian Atger, Meltem Weger, Cédric Gobet, Divya Ramnath, Aline Charpagne, Delphine Morin-Rivron, Elizabeth E. Powell, Matthew J. Sweet, Mojgan Masoodi, N. Henriette Uhlenhaut, and Frédéric Gachon

Correspondence: Frédéric Gachon
Email: f.gachon@uq.edu.au

This PDF file includes:

Other supplementary materials for this manuscript include the following:

Supplementary Information Text

SI Materials and Methods

Animal phenotyping

Mice were weighted every week, underwent several *in vivo* procedures (see below and figure S2A and S3C) and were sacrificed at ZT12 (ZT0 corresponds to the time when the light is switched on).

6-weeks old mice from the *Bmal1-Lep* line and 12-, 15-, 18-weeks old HFD or CD fed *Bmal1* KO and WT mice underwent body weight, size measurements and body fat content analysis using the Nuclear Magnetic Resonance technology with an EchoMRI^{TM}-700 analyzer at ZT 3. For each animal, the body mass index was calculated as the body weight (kg) divided by the square of the size (m).

10-weeks old mice from the *Bmal1-Lep* mice line and 12-, 15-, 18-weeks old HFD or CD fed *Bmal1* KO and WT mice underwent glycemia measurements (Breeze2 system, Bayer) after 15 hours fasting (ZT3) and after 6 hours refeeding (ZT9).

11-weeks old mice from the *Bmal1-Lep* line, 13-, 16-, 19-weeks old HFD or CD fed *Bmal1* KO and WT mice, and 9 weeks *Bmal1* HepKO mice underwent glucose tolerance tests at ZT3 after 15 hours fasting. Glycemia measurements (Breeze2 system, Bayer) were performed 0, 15, 30, 60, 90, 120 and 180 minutes after the intra-peritoneal injection of glucose (1g/kg).

12-weeks mice from the *Bmal1-Lep* line, 14-, 17-, 20-weeks HFD or CD fed *Bmal1* KO and WT mice, and 10 weeks *Bmal1* HepKO mice underwent insulin tolerance tests at ZT3. Glycemia measurements (Breeze2 system, Bayer) were performed 0, 15, 30, 60, 90, 120 and 180 minutes after the intra-peritoneal injection of insulin in both *Bmal1-Lep* and *Bmal1* mice lines (1 IU/kg and 0.5 IU/kg, respectively).

Histology

Liver and WAT pieces were fixed overnight in 10% formalin solution. Pieces were then washed three times in PBS solution. Liver slices underwent standard hematoxylin/eosin coloration and/or DAPI staining. For Oil-Red O staining, cryosections of liver were incubated in Oil-Red O solution followed by hematoxylin solution.

Serum chemistry analysis

Blood samples were collected, and sera were obtained after a centrifugation at 10 000 rpm for 10 min at room temperature. Sera were kept at -80°C until further analysis. Insulin, triglycerides, leptin, free testosterone and 17β-estradiol were measured accordingly to the protocols of the Mouse Insulin ELISA kit (Mercodia), the Triglycerides LabAssay kit (Wako), the Mouse Leptin ELISA kit (CrystalChem), the Testosterone ELISA kit (Enzo) and the Mouse/Rat Estradiol ELISA kit (Calbiotech), respectively.

Glycogen concentration

The liver glycogen extractions have been previously described (1). Briefly, frozen tissues were incubated 20 minutes at 100°C in 30% KOH solution. Ethanol 95% solution was added and a 20-minute centrifugation at 840g at 4°C allowed the precipitation of glycogen in a pellet. The glycogen was then diluted in water. After adding a 5% phenol solution and then 95-98% sulphuric acid, glycogen concentration was measured at the optic density 490 nm.

Liver lipids extraction and liver TAG measurements

Liver lipids were extracted as previously described (2). Briefly, frozen liver tissues were homogenized in an 30% alcoholic KOH solution at 60°C for 5 hours. After precipitation with 1M MgCl2 followed by a 30 min centrifugation at 14000 rpm, triglycerides content was measured using the Triglycerides LabAssay kit (Wako).

Lipid extraction and analysis

Approximately 10 mg of pulverized liver tissue was homogenized in 1 ml of 150 mM ammonium bicarbonate buffer using Tissue Lyser at a speed of 25 Hz for 2.5 min. Supernatant was removed into new glass tube on ice. 100 µl of the homogenate was collected and further diluted with 80 µl of 150 mM ammonium bicarbonate buffer using Hamilton Robot and 810 µl of MTBE /Methanol (7/2 v/v) containing internal standard was added to this mixture. The internal standard mixture contained: LPG 17:1, LPA 17:0, PC 17:0/17:0, PS 17:0/17:0, PG 17:0/17:0, PA 17:0/17:0, LPI 13:0, LPS 13:0, Chol D6, DAG 17:0/17:0, TAG 17:0/17:0/17:0, Cer 18:1;2/17:0, SM 18:1;2/12:0, LPC 12:0, LPE 17:1, PE 17:0/17:0, CE 20:0, PI 16:0/16:0. Solution was mixed at 700 rpm, 15 min at 4°C using a ThermoMixer C and then centrifugated at 3000 RCF for 5 min. 100 µl of the organic phase was transferred to a 96-well plate, dried in a speed vacuum concentrator. Lipid extract was reconstituted in 40 µl of 7.5 mM ammonium acetate in chloroform/methanol/propanol (1:2:4, V/V/V). All liquid handling steps were performed using Hamilton STAR robotic platform.

For MS data acquisition, samples were analyzed by direct infusion in a QExactive mass spectrometer (Thermo Fisher Scientific) equipped with a TriVersa NanoMate ion source (Advion Biosciences). Samples were acquired in both polarity modes in a single acquisition at Rm/z=200=140000. All data was analyzed with in-house developed lipid identification software based on LipidXplorer. Abundance of lipids was normalized by tissue weight. The statistical analysis followed a two-step procedure. Only for lipids that have been measured in 50% or more samples in each genotype, a linear model was fitted and applied to the normalized log2-transformed lipid levels. We used the anova() function to compare a full model (with the explanatory variable genotype) and reduced model with only an intercept to identify lipids that are significantly different across genotypes. Subsequently, we contrast all possible combination of genotypes within the linear model. Finally,

P-values were corrected for multiple testing using stageR (3) with the ANOVA result used during the screening stage, while P-values of the individual contrasts were used in the confirmation stage.

Realtime QPCR

0.5 µg of liver RNA was reverse transcribed using random hexamers and SuperScript II reverse transcriptase (Life Technologies). The cDNAs equivalent to 20 ng of RNA were PCR amplified in a LightCycler 480 II (Roche) using the TaqMan technology. In each independent experiment, *Cidec* gene expression (Mm00617672_m1, Thermo Fisher Scientific) is normalized by *Gapdh* mRNA (Mm 99999915_g1).

RNA-sequencing and analysis

RNA was quantified with Ribogreen (Life Technologies) and quality assessed on a Fragment Analyzer (Advances Analytical). Sequencing libraries were prepared from 250 ng total RNA using the TruSeq Stranded RNA Sample Prep Kit v2 (Illumina) with the Ribo-Zero Gold depletion set. The procedure was automated on a Sciclone NGS Workstation (Perkin Elmer). We followed the manufacturer's protocol except for the PCR amplification step. The latter was run for 12 cycles with the KAPA HiFi HotStart ReadyMix (Kapa BioSystems). The optimal PCR cycle number has been evaluated using the Cycler Correction Factor method as previously described (4). Purified libraries were quantified with Picogreen (Life Technologies) and the size pattern was controlled with the DNA High Sensitivity Reagent kit on a LabChip GX (Perkin Elmer). Libraries were then pooled by 18 and each pool was clustered at a concentration of 10 pmol on 4 lanes of two High Output (8-lane) v3 flow cell (Illumina). Paired-end sequencing was performed for 2 x 100 cycles on a HiSeq 2500. RNA-Seq data for human liver biopsies of patients with obesity or a range of clinicopathologic conditions including steatohepatitis with or without mild inflammation (NAFLD) or a necroinflammatory subtype, NASH, and patients with chronic hepatitis C with varying stages of fibrosis (fibrosis stages 0-4) were retrieved from GEO (GSE126848) (5) and ENA (PRJEB27201) (6), repectively. RNA-Seq data from *Bmal1* WT and *Bmal1* KO mice collected across the course of a day were retrieved from GEO (GSE73554) (7). The data for male and female C57BL/6 mice has been downloaded from accession number GSE114400 (8) at GEO.

We used STAR 2.4.0i (9) to map reads onto the Ensembl *Mus musculus* (GRCm38/mm10) or *Homo sapiens* (GRCh38/hg38) genome and to quantify the number of reads per gene. The differential gene expression analysis for the four mouse genotypes (i.e., WT-WT, KO-WT, WT-Ob, KO-Ob) was performed using a two-step procedure. Firstly, we used a global likelihood ratio test (LRT) within the DESeq2 framework (10) to assess genes that are differential expressed between any genotype. Secondly, we contrast all possible combination of genotypes. *P*-values were corrected using stageR (3) using the result of the LRT in the screening stage and and the *P*-values of the individual contrasts in the confirmation stage. The three tissues

(i.e., muscle, eWAT and liver) were analysed separately. As the liver samples from *Bmal1* WT, *Bmal1* KO, *Bmal1* HepWT, and *Bmal1* HepKO data have been sampled around the course of a day, we used dryR (11) to assess the mean differences between the conditions.

We employed DESeq2 for differential gene expression analysis in the human datasets (10). To determine genes that are differentially expressed in humans with increasing stage of fibrosis (stages 0-4; dataset 2), we also used a LRT. Age, sex, and time of biopsy was included in our statistical model as covariates (Dataset S1). As the information of timing was not available for human liver biopsies of subjects with varying severity of NAFLD (dataset 1) and the study design was not sex balanced, we included only male subjects into the analysis and age as covariate statistical model. To determine female-biased and male-biased genes in human liver, we contrasted male and female subjects showing no signs of fibrosis (stage 0) using dataset 2. As most female subjects showed low or no signs of liver fibrosis in dataset 2, we restricted the analysis of sexual dimorphism to male subjects only (Fig. 6). In this case the statistical model included age, and time of biopsy as covariates. Multiple testing was corrected by the Benjamini-Hochberg procedure for the mouse and human data (12).

Functional and Gene Set-Enrichment Analysis

For the mouse RNA-seq datasets, we tested enrichment for annotated gene sets from Gene Ontology (GO) (13) and focused on biological processes. We used GOseq 3.1 (14) to calculate overrepresentation of gene sets for genes assigned to a statistical model (Dataset S4 and S6). Only GO terms with a significant enrichment p-value < 0.01 are presented in the Datasets.

Transcription factor activity analysis

To predict transcription factor binding sites in human promoters of differentially expressed genes, we employed MotEvo (15) and scanned $\pm$ 500 bp around the annotated transcription start site (TSS) of a gene. TSS definition were retrieved from (16) and weight matrices were downloaded from Swiss regulon (17). Target genes for AR, ESR1, and MYOD1 in mouse have been identified using published ChIP-Seq (Table S1). We mapped reads on the Ensembl *M. musculus* genome (GRCm38/mm10) using STAR-2.7.3a (9). Peaks were called using macs/2-2.1.1 (18) and peak annotation was performed with ChIPseeker 3.10 with a distance from TSS of $\pm$ 5 kb (19) using the genome annotation of Ensembl release 98 (20). Female and male STAT5 targets were taken from (21). Female and male biased genes in mouse liver were identified in (22). To predict activities (Z-score activity) of transcription factors and male and female biased genes in the human and mouse datasets, we applied ISMARA, a tool that is based on a penalized regression model which uses an L2 penalty (23).

Table S1. ChIP-Seq data used for the analysis of transcription factor activity

RESOURCES	SOURCE	IDENTIFIER
Raw data; ChIP-seq AR (epididymis)	GEO (http://www.ncbi.nlm.nih.gov/geo/)	GEO: GSE121151 (24)
Raw data; ChIP-seq ESR1 (female liver)	GEO (http://www.ncbi.nlm.nih.gov/geo/)	GEO: GSE49993 (25)
Raw data; ChIP-seq ESR1 (uterus)	GEO (http://www.ncbi.nlm.nih.gov/geo/)	GEO: GSE125972 (26)
Raw data; ChIP-seq MYOD1 (C2C12 myoblasts)	GEO (http://www.ncbi.nlm.nih.gov/geo/)	GEO: GSE49313 (27)

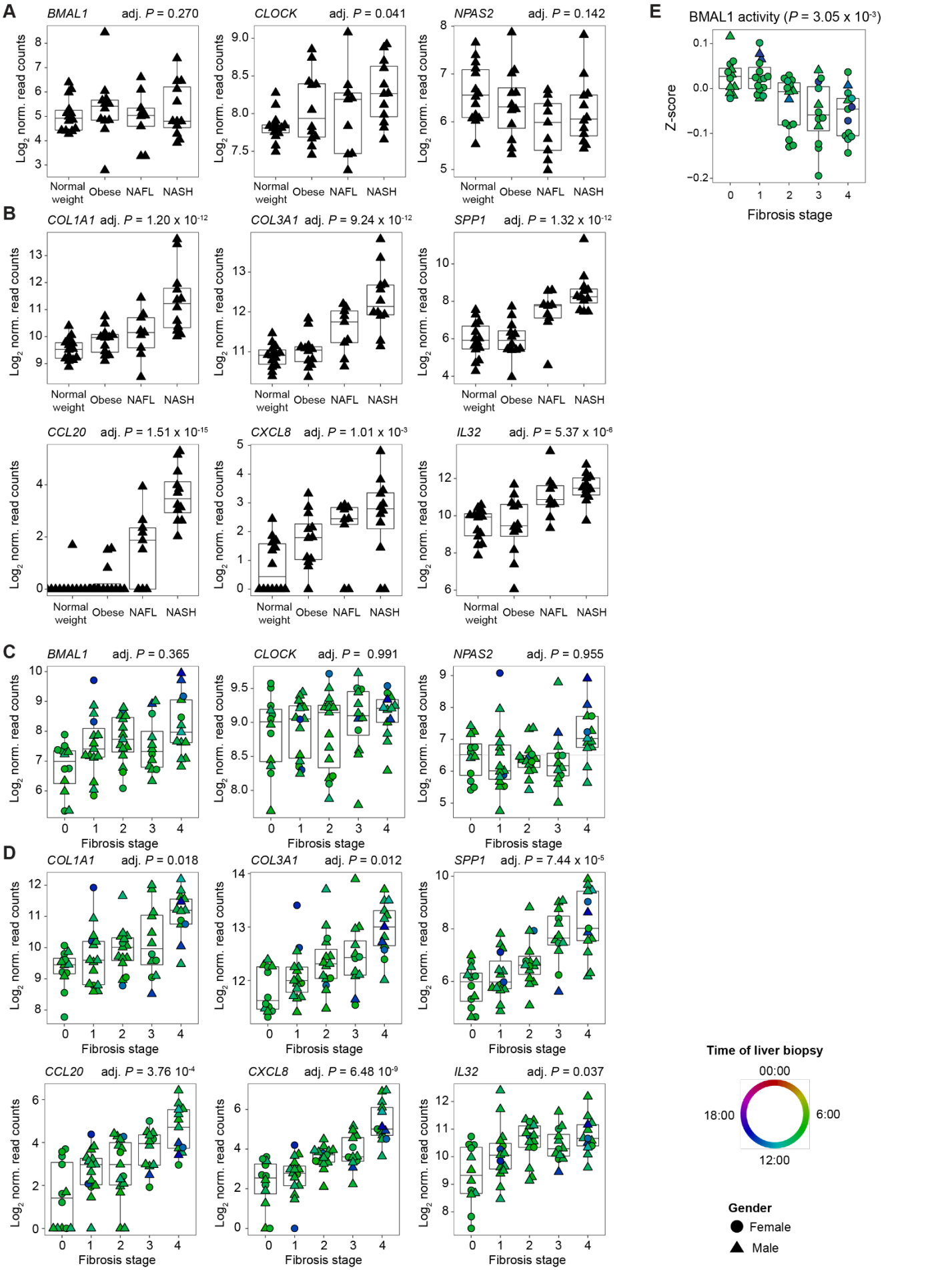
A
BMAL1 adj. P = 0.270
CLOCK adj. P = 0.041
NPAS2 adj. P = 0.142
B
COL1A1 adj. P = 1.20 x 10-12
COL3A1 adj. P = 9.24 x 10-12
SPP1 adj. P = 1.32 x 10-12
CCL20 adj. P = 1.51 x 10-15
CXCL8 adj. P = 1.01 x 10-3
IL32 adj. P = 5.37 x 10-6
C
BMAL1 adj. P = 0.365
CLOCK adj. P = 0.991
NPAS2 adj. P = 0.955
D
COL1A1 adj. P = 0.018
COL3A1 adj. P = 0.012
SPP1 adj. P = 7.44 x 10-5
CCL20 adj. P = 3.76 10-4
CXCL8 adj. P = 6.48 10-9
IL32 adj. P = 0.037
Log2 norm. read counts
Normal weight
Obese
NAFL
NASH
Fibrosis stage
E
BMAL1 activity (P = 3.05 x 10-3)
Z-score
Time of liver biopsy
00:00
6:00
12:00
18:00
Gender
Female
Male

Figure S1: Regulation of BMAL1 activity in obesity and liver diseases in humans

A, B. Expression of *BMAL1* and its heterodimerization partners (A) and genes related to inflammation or fibrosis (B) in the liver of humans with normal weight, obesity or liver diseases. $n \geq 9$ subjects per condition.
C, D. Expression of *BMAL1* and its heterodimerization partners (C) and genes related to inflammation or fibrosis (D) in the liver of humans at different stages of fibrosis. $n \geq 12$ subjects per stage.
E. Predicted activity of BMAL1 in the liver of individuals at different stage of fibrosis.
Color code represents the time of liver biopsy.
P-values were determined with a generalized linear model (for details see Material and Methods).

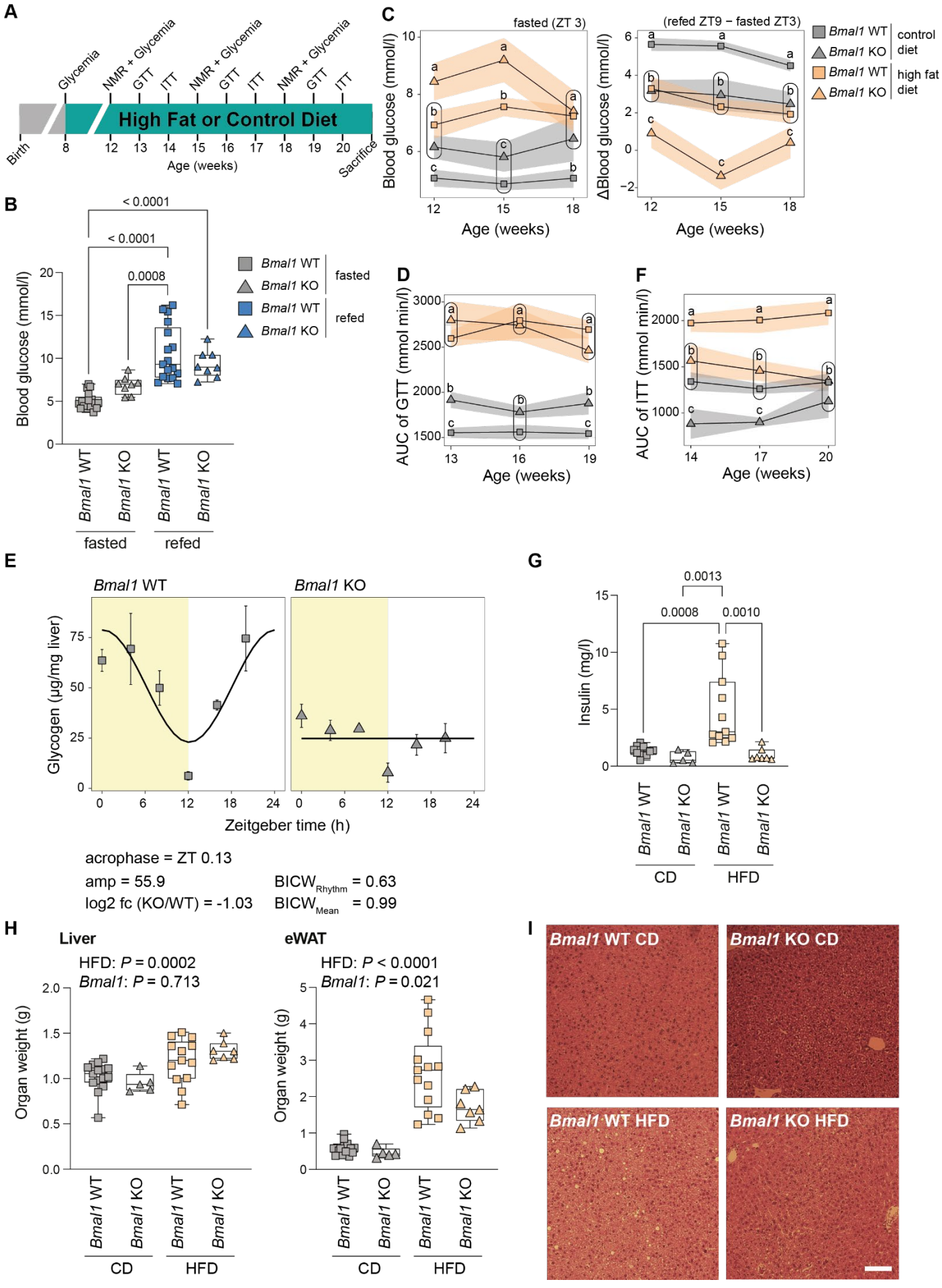
A
Glycemia
NMR + Glycemia
GTT
ITT
NMR + Glycemia
GTT
ITT
NMR + Glycemia
GTT
ITT
High Fat or Control Diet
Birth
8
12
13
14
15
16
17
18
19
20
Sacrifice
Age (weeks)
B
< 0.0001
< 0.0001
0.0008
Blood glucose (mmol/l)
Bmal1 WT
Bmal1 KO
Bmal1 WT
Bmal1 KO
fasted
refed
Bmal1 WT
Bmal1 KO
fasted
Bmal1 WT
Bmal1 KO
refed
C
fasted (ZT 3)
(refed ZT9 − fasted ZT3)
Blood glucose (mmol/l)
ΔBlood glucose (mmol/l)
Age (weeks)
Age (weeks)
Bmal1 WT
Bmal1 KO
control diet
Bmal1 WT
Bmal1 KO
high fat diet
D
AUC of GTT (mmol min/l)
Age (weeks)
F
AUC of ITT (mmol min/l)
Age (weeks)
E
Bmal1 WT
Bmal1 KO
Glycogen (µg/mg liver)
Zeitgeber time (h)
acrophase = ZT 0.13
amp = 55.9
log2 fc (KO/WT) = -1.03
BICW Rhythm = 0.63
BICW Mean = 0.99
G
0.0013
0.0008
0.0010
Insulin (mg/l)
Bmal1 WT
Bmal1 KO
Bmal1 WT
Bmal1 KO
CD
HFD
H
Liver
HFD: P = 0.0002
Bmal1: P = 0.713
eWAT
HFD: P < 0.0001
Bmal1: P = 0.021
Organ weight (g)
Organ weight (g)
Bmal1 WT
Bmal1 KO
Bmal1 WT
Bmal1 KO
CD
HFD
I
Bmal1 WT CD
Bmal1 KO CD
Bmal1 WT HFD
Bmal1 KO HFD

Figure S2: *Bmal1* KO mice under HFD exhibit an early obese phenotype but no sign of prediabetes

A. Schematic of the experimental protocol used for *Bmal1* KO and their WT littermates under control (CD) and high fat (HFD) diet. 8 weeks old mice underwent glycemia measurement after 15 hours of fasting and after 6 hours of refeeding. Then, the mice were placed under CD or HFD for 12 weeks. During this period, glycemia, glucose and insulin tolerances were assayed every 3 weeks according to the schedule.
B. Glycemia of *Bmal1* KO and WT mice under regular chow diet after 15 hours of fasting (ZT3) and after 6 hours of refeeding (ZT9). n = 8-17 mice per condition.
C. Evolution of blood glucose concentration after 15 hours of fasting (ZT3, left) and after 6 hours of refeeding (ZT9, right) during the experiment with CD or HFD. The differences in blood glucose were compared to fasting values. n = 7-19 mice per condition and week.
D. Area under the curve related to the glucose tolerance tests (Fig 2F) performed on 13, 16, and 19 weeks-old mice at ZT3 after 15 hours of fasting. n = 6-17 mice per condition and week.
E. Temporal glycogen concentration in *Bmal1* KO and WT mice liver under CD. The Zeitgeber Time (ZT) is defined as followed: ZT0 lights on; ZT12: lights off. n = 3 per time point and genotype.
F. Area under the curve related to the insulin tolerance tests (Fig 2G) performed on 14, 17, and 20 weeks-old mice at ZT3. n = 4-14 mice per condition and week.
G. Circulating insulin concentration in *Bmal1* KO and WT under CD and HFD conditions at ZT12. n = 5-12 mice per condition.
H. Liver (left) and eWAT (right) weight from *Bmal1* KO and WT mice under CD or HFD at ZT12. n = 5-15 mice per condition.
I. Representative liver sections stained with hematoxylin and eosin from *Bmal1* KO and WT mice under CD or HFD at ZT12. The scale bar corresponds to 50 μm.
Statistical tests included linear models (C, D, and F; see details in methods), two-way ANOVA (H followed by a Holm-Sídák multiple comparison test (B, and H), and *dryR* (E). Means with different letters significantly differ ($P < 0.05$; C, D, and F).

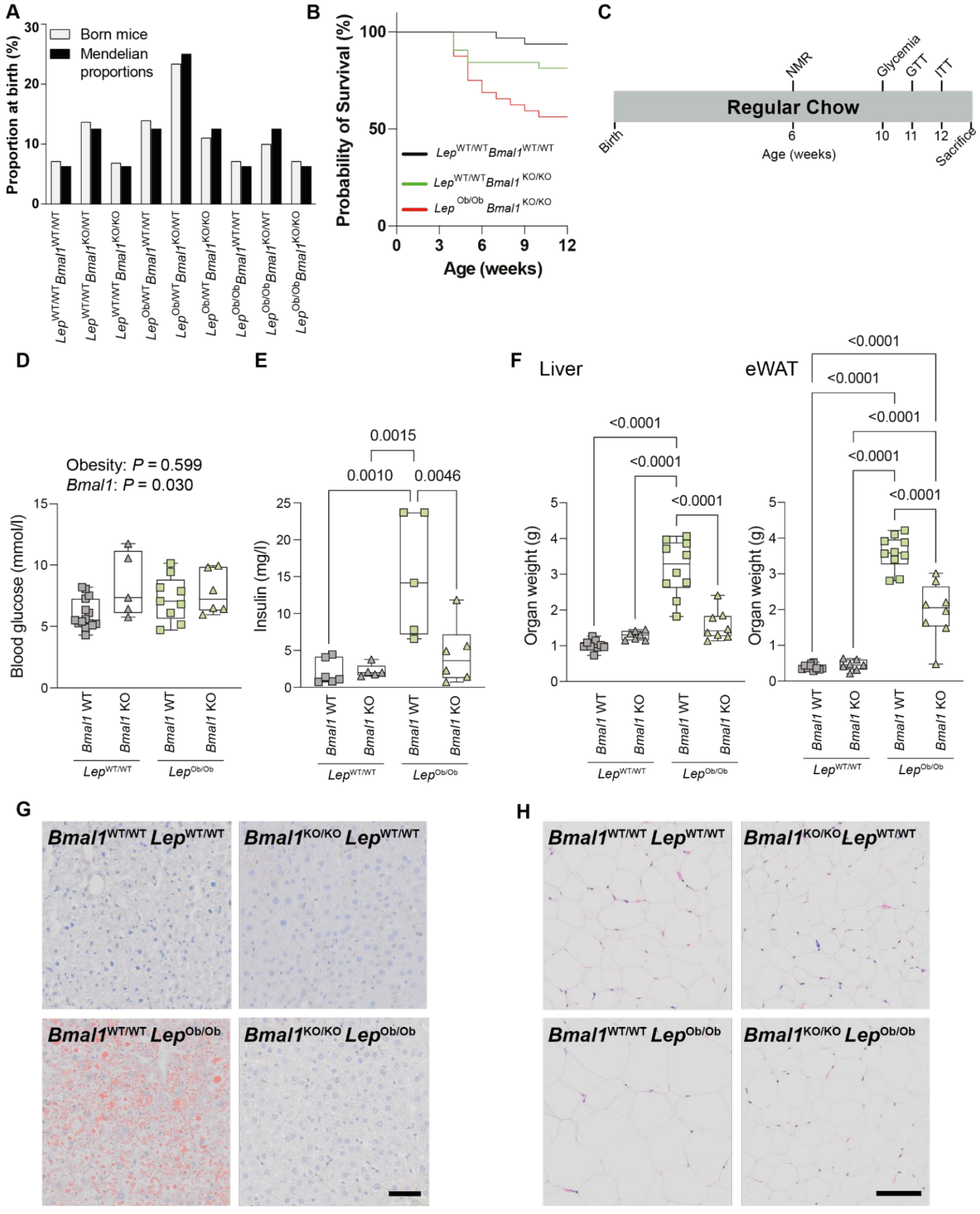
A
Proportion at birth (%)
Born mice
Mendelian proportions
B
Probability of Survival (%)
Age (weeks)
C
NMR
Glycemia
GTT
ITT
Regular Chow
Birth
Age (weeks)
Sacrifice
D
Obesity: P = 0.599
Bmal1: P = 0.030
Blood glucose (mmol/l)
E
Insulin (mg/l)
0.0015
0.0010
0.0046
F
Liver
eWAT
Organ weight (g)
<0.0001
G
H

Figure S3: Consequences of *Bmal1* deletion in the absence of leptin

A. Distribution of the mice born per genotype compared to the expected mendelian proportions. The cohort consisted of a total of n = 504 mice.
B. Survival curve for *Bmal1*$^{WT/WT}$-*Lep*$^{WT/WT}$, *Bmal1*$^{KO/KO}$-*Lep*$^{WT/WT}$, and *Bmal1*$^{KO/KO}$-*Lep*$^{Ob/Ob}$ littermates. n = 32-33 mice per genotype.
C. Schematic of the experimental protocol used for the *Bmal1-Lep* mice line. Analyses of the body composition by EchoMRI were performed on 6 weeks old mice. The mice underwent glycemia measurements after 15 hours of fasting and after 6 hours of refeeding (week 10), glucose and insulin tolerances were assayed at the age of 11 and 12 weeks, respectively. The organs were harvested and weighted on 13 weeks old mice at ZT12.
D. Glycemia of the animals of the four genotypes after 15 hours of fasting (ZT3). n = 5-15 mice per genotype
E. Circulating insulin concentration in the animals of the four genotypes at ZT12. n = 5-6 mice per genotype.
F. Liver (left) and eWAT (right) weight from animals of the four genotypes at ZT12. n = 7-10 mice per genotype
G. Representative liver sections stained with oil red O from animals of the four genotypes. The scale bar corresponds to 50 µm.
H. Representative eWAT sections stained with hematoxylin and eosin from animals of the four genotypes. The scale bar corresponds to 100 µm.
P-values were determined by a two-way ANOVA (D–F) followed by a Holm-Šídák multiple comparison test if interaction term was significant ($P < 0.05$). *P*-values below 0.05 are provided indicated.

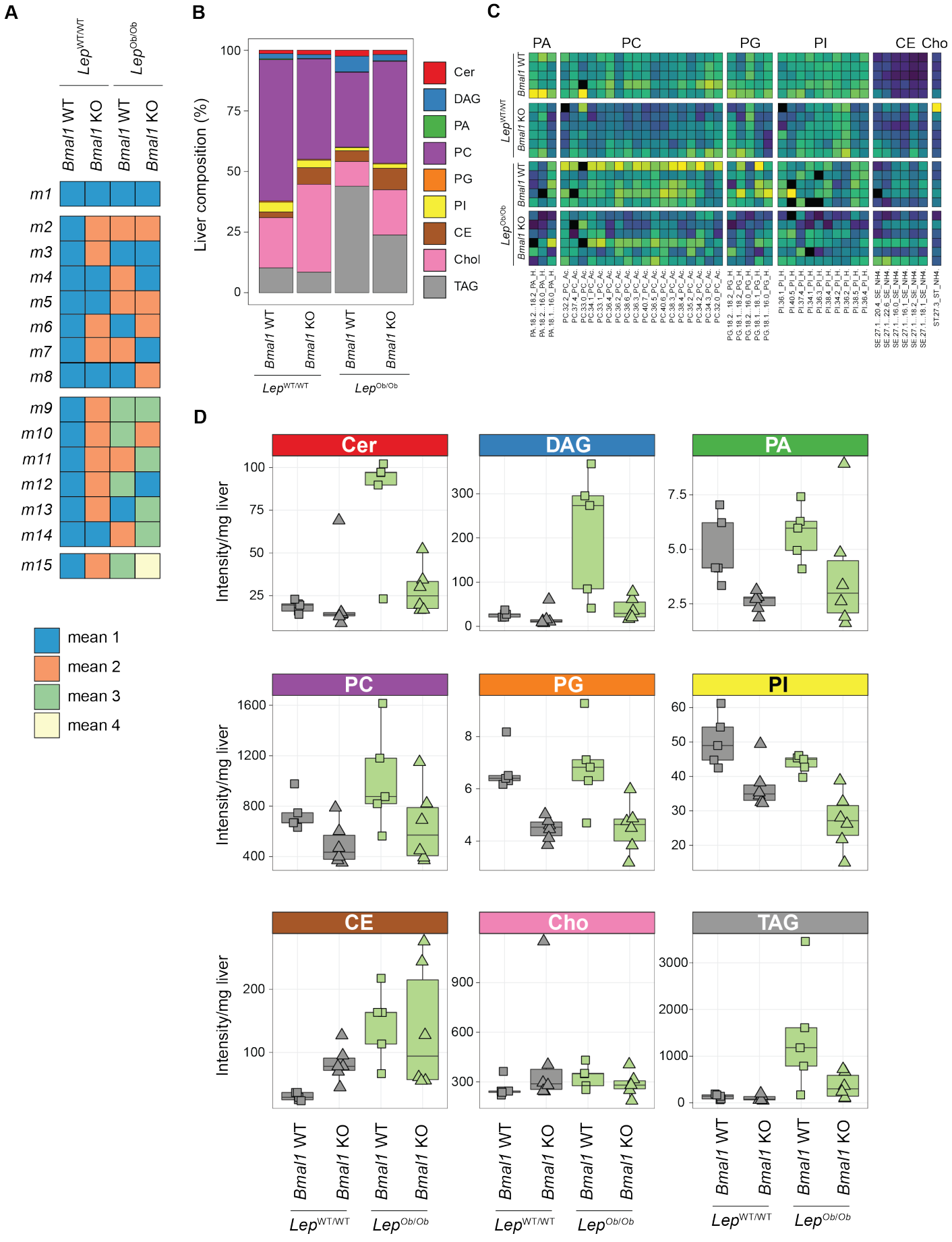
A
Lep^WT/WT
Lep^Ob/Ob
Bmal1 WT
Bmal1 KO
Bmal1 WT
Bmal1 KO
m1
m2
m3
m4
m5
m6
m7
m8
m9
m10
m11
m12
m13
m14
m15
mean 1
mean 2
mean 3
mean 4
B
Liver composition (%)
100
75
50
25
0
Cer
DAG
PA
PC
PG
PI
CE
Chol
TAG
Bmal1 WT
Bmal1 KO
Bmal1 WT
Bmal1 KO
Lep^WT/WT
Lep^Ob/Ob
C
PA
PC
PG
PI
CE
Cho
Lep^WT/WT
Lep^Ob/Ob
Bmal1 WT
Bmal1 KO
Bmal1 WT
Bmal1 KO
D
Cer
DAG
PA
PC
PG
PI
CE
Cho
TAG
Intensity/mg liver
Bmal1 WT
Bmal1 KO
Bmal1 WT
Bmal1 KO
Lep^WT/WT
Lep^Ob/Ob

Figure S4: BMAL1 controls of lipid metabolism and storage

A. Overview of all models that are fitted in case the data consists of four conditions. Same color indicates shared mean levels between indicated conditions.
B. Global liver lipids relative composition analyzed by lipidomics in each group of mice liver at ZT12. Values represent average of n = 5-6 mice per genotype. TAG: triacylglycerides, Chol: cholesterol, CE: cholesteryl esters, PI: phosphatidylinositols, PG: phosphatidylglycerols, PC: phosphatidylcholines, PA: phosphatidic acid, DAG: diacylglycerides, Cer: ceramides.
C. Heatmap of specific lipid species (PA, PC, PG, PI, CE, and Chol) abundance in liver of individual mice.
D. Accumulation of family liver of lipid species at ZT12. n = 4-6 mice per genotype.

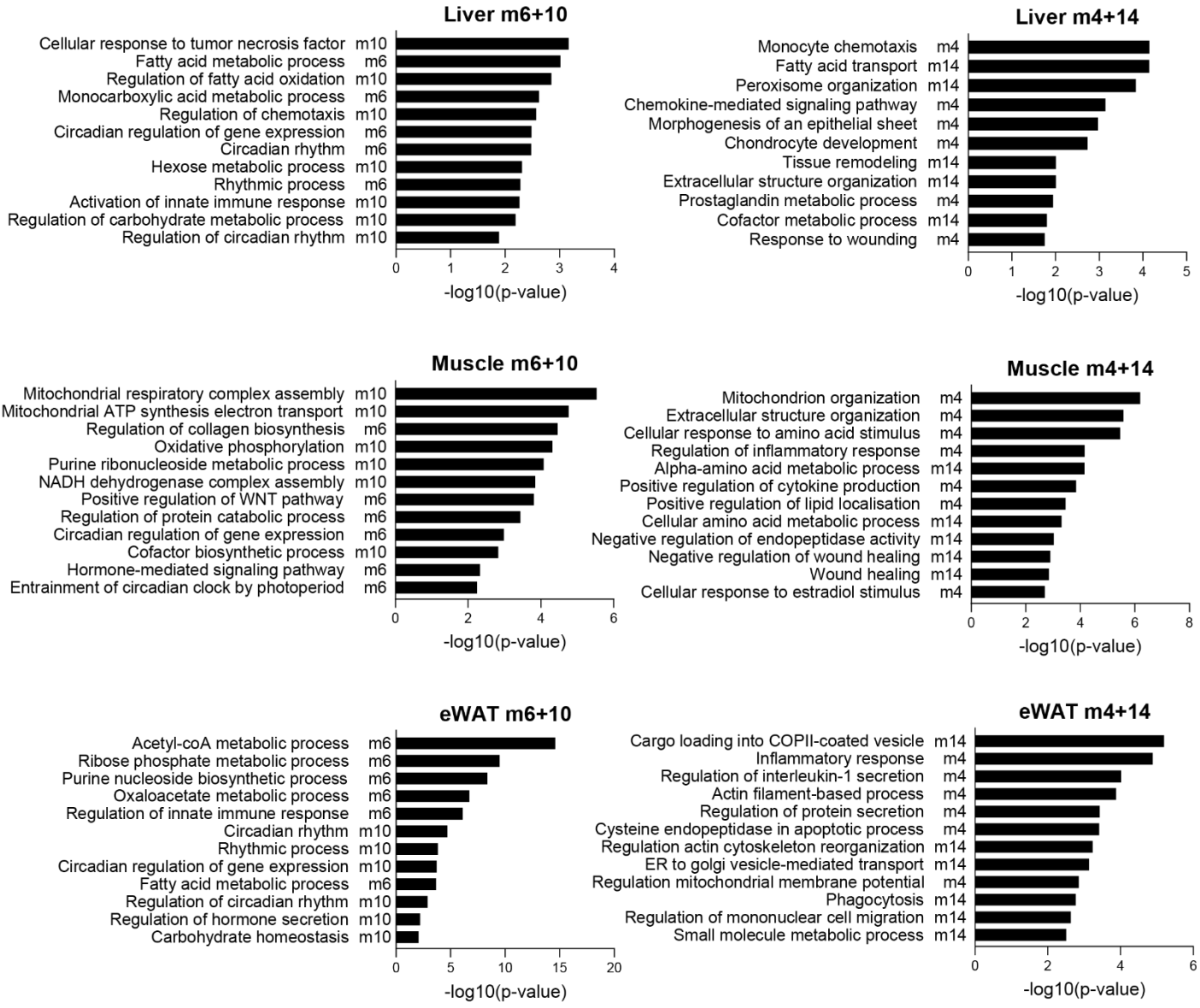

Figure S5: Most overrepresented biological processes impacted by the deletion of *Bmal1* and leptin deficiency in the liver, muscle, and eWAT

Representative biological processes associated with differential expressed genes between WT and *Bmal1* KO mice irrespective of their leptin status (models 6 and 10, left) or differentially expressed specifically in WT-Ob mice (models 4 and 14, right) in the liver (top panels), skeletal muscle (middle panels), or eWAT (bottom panels). Only biological processes with number of genes lower than 500 are represented to exclude housekeeping biological processes. The full list of pathways can be found in Dataset S4.

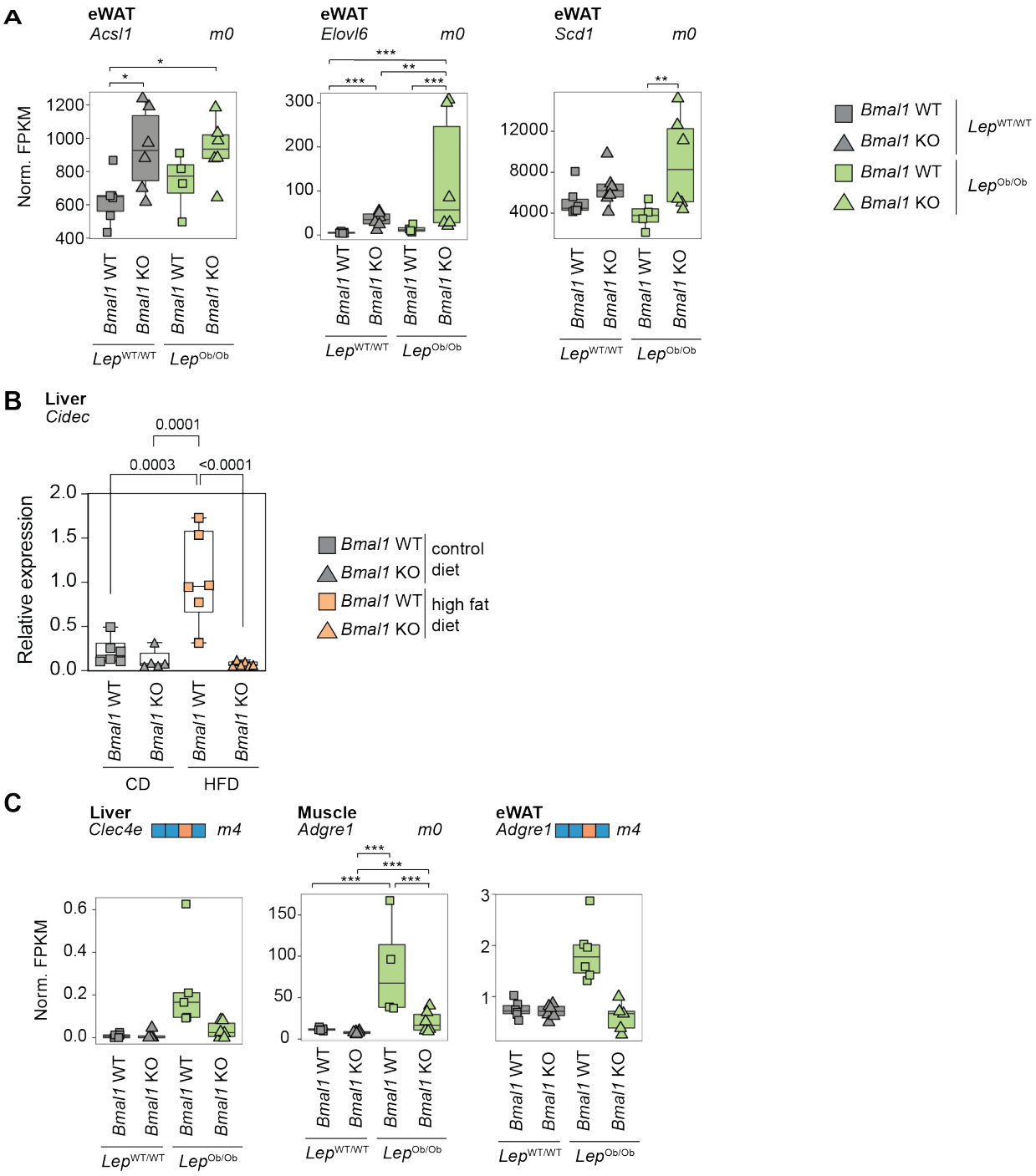

Figure S6: Impact of the deletion of *Bmal1* on lipid metabolism and inflammation

A. Expression of genes encoding enzymes involved in lipid metabolism measured by RNA-Seq at ZT12 in eWAT. n = 4-6 mice per genotype.
B. Relative *Cidec* gene expression in liver from *Bmal1* KO and WT mice under CD and HFD condition at ZT12. n = 5-6 mice per genotype.
C. Expression of markers of the infiltration of immune cells measured by RNA-Seq at ZT12 in liver (left), muscle (middle) and eWAT (right). n = 4-6 mice per genotype.
Statistical tests included generalized linear models (A, and C, see details in methods) and a two-way ANOVA (B) followed by a Holm-Sidak multiple comparison test. Differences in expression levels between the genotypes (A, and C) are defined in Figure S4A and are indicated on top of the graphs.

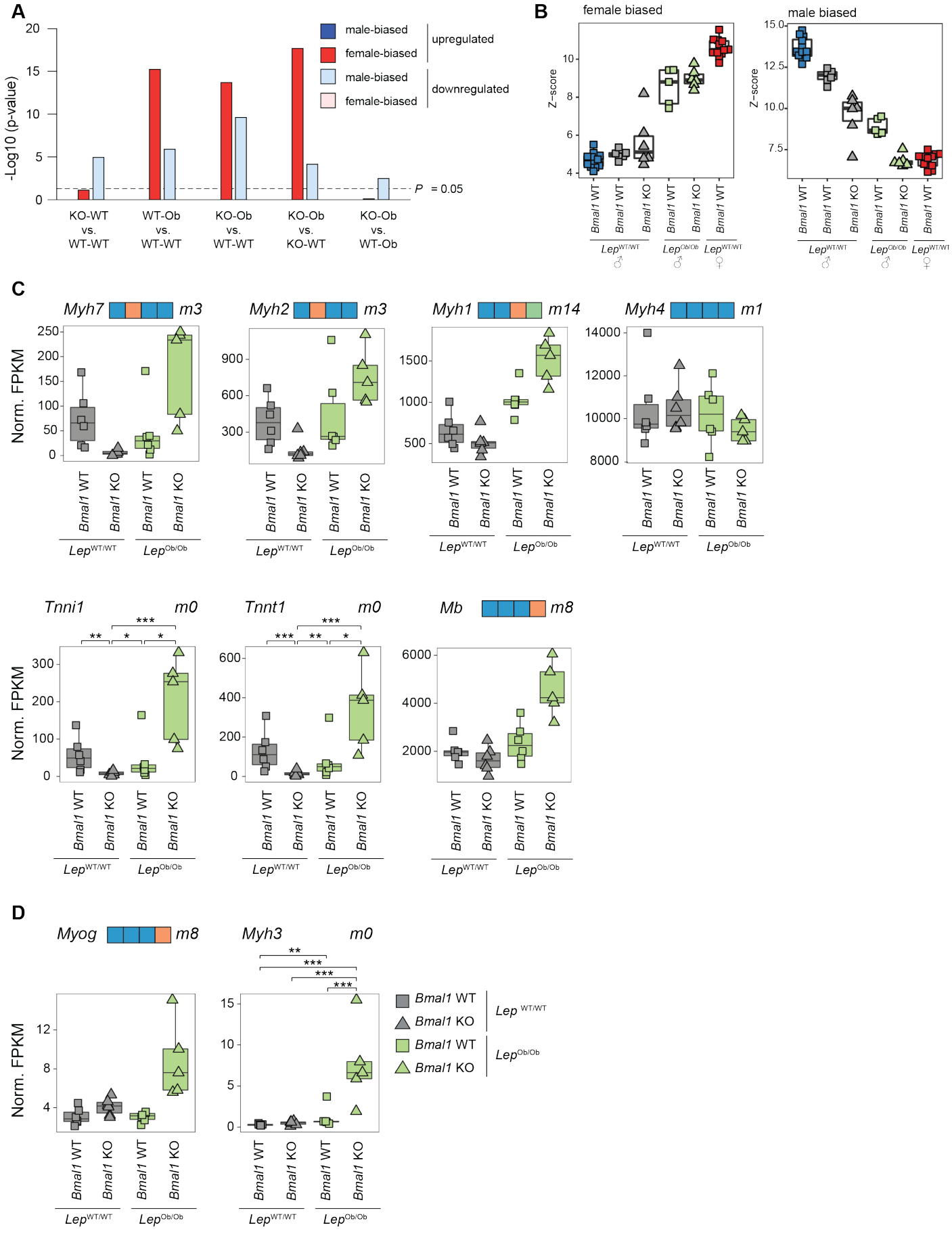
A
-Log10 (p-value)
male-biased
female-biased
male-biased
female-biased
upregulated
downregulated
P = 0.05
KO-WT vs. WT-WT
WT-Ob vs. WT-WT
KO-Ob vs. WT-WT
KO-Ob vs. KO-WT
KO-Ob vs. WT-Ob
B
female biased
male biased
Z-score
Bmal1 WT
Bmal1 KO
Lep WT/WT
Lep Ob/Ob
C
Myh7 m3
Myh2 m3
Myh1 m14
Myh4 m1
Norm. FPKM
Tnni1 m0
Tnnt1 m0
Mb m8
D
Myog m8
Myh3 m0
Bmal1 WT
Bmal1 KO
Lep WT/WT
Lep Ob/Ob

Figure S7: Gene expression analysis revealed the impact of *Bmal1* deletion on feminization of gene expression and muscle physiology

A. Statistical analysis of male- and female-biased genes showing a significant differential gene expression of sex-biased genes in the different genotype comparisons. n = 5-6 mice per genotype.
B. Comparison of hepatic female- and male-biased genes in differential expressed genes between the four genotypes (replicated from Figure 5A) with male and female C57BL/6 mice (raw data from (22)). n = 5-12 mice per genotype.
C. Expression of genes encoding muscle fiber types-specific myosin heavy chains or slow type-specific Troponin and Myoglobin measured by RNA-Seq at ZT12 in muscle. n = 5-6 mice per genotype.
D. Expression of markers of muscle regeneration measured by RNA-Seq at ZT12 in muscle. n = 5-6 mice per genotype.
Statistical tests included a mean-rank gene set enrichment analysis (A), and generalized linear models (C, and D, see details in methods). Differences in expression levels between the genotypes (C, and D) are defined in Figure S4A and are indicated on top of the graphs. Genes that follow an ambiguous model are marked *m0* and *P*-values for each significant contrast are provided. $***$ $P < 0.001$, $**$ $P < 0.01$, and $*$ $P < 0.05$.

Legends for Datasets S1 to S6 (Separate files)

Dataset S1. RNA-Seq Analysis results of liver biopsies of chronic liver disease patients
Sheet 1. Detailed table legend.
Sheet 2. Results of the differential analysis in normal, obese, NAFL, and NASH patients (dataset 1).
Sheet 3. Results of the differential expression analysis in liver biopsies of chronic liver disease patients with varying fibrosis stage (dataset 2).
Sheet 4. Sample annotations of dataset 2 including time of liver biopsy.
Sheet 5. Results of the differential expression analysis between liver biopsies of non-fibrotic male vs. female subjects (dataset 2).

Dataset S2. Liver lipidomics results and analysis from *Bmal1*$^{KO/KO}$-*Lep*$^{Ob/Ob}$ (KO-Ob), *Bmal1*$^{KO/KO}$-*Lep*$^{WT/WT}$ (KO-WT), *Bmal1*$^{WT/WT}$-*Lep*$^{Ob/Ob}$ (WT-Ob), and *Bmal1*$^{WT/WT}$-*Lep*$^{WT/WT}$ (WT-WT) mice
Sheet 1. Detailed table legend.
Sheet 2. Results of the differential analysis in liver.

Dataset S3. RNA-Seq results and analysis of *Bmal1*$^{KO/KO}$-*Lep*$^{Ob/Ob}$ (KO-Ob), *Bmal1*$^{KO/KO}$-*Lep*$^{WT/WT}$ (KO-WT), *Bmal1*$^{WT/WT}$-*Lep*$^{Ob/Ob}$ (WT-Ob), and *Bmal1*$^{WT/WT}$-*Lep*$^{WT/WT}$ (WT-WT) mice in liver, muscle, and eWAT
Sheet 1. Detailed table legend.
Sheet 2. Results of the differential expression analysis using DESeq2 in liver.
Sheet 3. Results of the differential expression analysis using DESeq2 in muscle.
Sheet 4. Results of the differential expression analysis using DESeq2 in eWAT.

Dataset S4. GO terms associated with differentially expressed genes in *Bmal1*$^{KO/KO}$-*Lep*$^{Ob/Ob}$ (KO-Ob), *Bmal1*$^{KO/KO}$-*Lep*$^{WT/WT}$ (KO-WT), *Bmal1*$^{WT/WT}$-*Lep*$^{Ob/Ob}$ (WT-Ob), and *Bmal1*$^{WT/WT}$-*Lep*$^{WT/WT}$ (WT-WT) liver, muscle, and eWAT
Sheet 1. Detailed table legend.
Sheet 2. Biological Process associated with differential expressed genes in liver.
Sheet 3. Biological Process associated with differential expressed genes in muscle.
Sheet 4. Biological Process associated with differential expressed genes in eWAT.

Dataset S5. RNA-Seq results and analysis of liver gene expression in hepatocyte specific *Bmal1*$^{KO/KO}$ (*Bmal1* HepKO) and wild-type (*Bmal1* HepWT) controls
Sheet 1. Detailed table legend.
Sheet 2. Results of the differential expression analysis using DESeq2.

Dataset S6. GO terms associated with differentially expressed genes of *Bmal1*$^{WT/WT}$ (*Bmal1* WT), *Bmal1*$^{KO/KO}$ (*Bmal1* KO) and hepatocyte specific *Bmal1*$^{KO/KO}$ (*Bmal1* HepKO) and wild-type (*Bmal1* HepWT) controls in liver.
Sheet 1. Detailed table legend.
Sheet 2. Biological Process associated with differential expressed genes (model 5) in liver.
Sheet 3. Biological Process associated with differential expressed genes (model 6) in liver.
Sheet 4. Biological Process associated with differential expressed genes (model 7) in liver.
Sheet 5. Biological Process associated with differential expressed genes (model 9) in liver.
Sheet 6. Biological Process associated with differential expressed genes (model 10) in liver.
Sheet 7. Biological Process associated with differential expressed genes (model 11) in liver.
Sheet 8. Biological Process associated with differential expressed genes (model 12) in liver.
Sheet 9. Biological Process associated with differential expressed genes (model 13) in liver.
Sheet 10. Biological Process associated with differential expressed genes (model 14) in liver.
Sheet 11. Biological Process associated with differential expressed genes (model 15) in liver.

SI References

1. S. Lo, J. C. Russell, A. W. Taylor, Determination of glycogen in small tissue samples. *J Appl Physiol* **28**, 234-236 (1970).
2. C. B. Peek *et al.*, Circadian Clock NAD^+ Cycle Drives Mitochondrial Oxidative Metabolism in Mice. *Science* **342**, 1243417 (2013).
3. K. Van den Berge, C. Soneson, M. D. Robinson, L. Clement, stageR: a general stage-wise method for controlling the gene-level false discovery rate in differential expression and differential transcript usage. *Genome Biol* **18**, 151 (2017).
4. F. Atger *et al.*, Circadian and feeding rhythms differentially affect rhythmic mRNA transcription and translation in mouse liver. *Proc Natl Acad Sci U S A* **112**, E6579-E6588 (2015).
5. K. Rigbolt, J. C. Nielsen, Hepatic transcriptome signatures in patients with varying degrees of non-alcoholic fatty liver disease compared to healthy normal-weight individuals. *Gene Expression Omnibus (GEO)*, https://www.ncbi.nlm.nih.gov/geo/query/acc.cgi?acc=GSE126848 (2019).
6. I. f. M. Bioscience, I. C. f. I. a. D. Research, RNA-seq of hepatic biopsies taken from patients with chronic liver disease presenting with different aetiologies (HCV, FLD) and fibrosis stages. *European Nucleotide Archive (ENA)*, https://www.ebi.ac.uk/ena/browser/view/PRJEB27201 (2018).
7. F. Atger *et al.*, Circadian and feeding rhythms differentially affect rhythmic mRNA transcription and translation in mouse liver. *Gene Expression Omnibus (GEO)*, https://www.ncbi.nlm.nih.gov/geo/query/acc.cgi?acc=GSE73554 (2015).
8. B. D. Weger *et al.*, Temporal profiles of germ-free and conventionally raised female and male mice. *Gene Expression Omnibus (GEO)*, https://www.ncbi.nlm.nih.gov/geo/query/acc.cgi?acc=GSE114400 (2018).
9. A. Dobin *et al.*, STAR: ultrafast universal RNA-seq aligner. *Bioinformatics* **29**, 15-21 (2013).
10. M. Love, W. Huber, S. Anders, Moderated estimation of fold change and dispersion for RNA-seq data with DESeq2. *Genome Biol* **15**, 550 (2014).
11. B. D. Weger *et al.*, Systematic analysis of differential rhythmic liver gene expression mediated by the circadian clock and feeding rhythms. *Proc Natl Acad Sci U S A* **118**, e2015803118 (2021).
12. Y. Benjamini, Y. Hochberg, Controlling the False Discovery Rate: A Practical and Powerful Approach to Multiple Testing. *J R Statist Soc B* **57**, 289-300 (1995).
13. M. Ashburner *et al.*, Gene Ontology: tool for the unification of biology. *Nat Genet* **25**, 25-29 (2000).
14. M. D. Young, M. J. Wakefield, G. K. Smyth, A. Oshlack, Gene ontology analysis for RNA-seq: accounting for selection bias. *Genome Biol* **11**, R14 (2010).
15. P. Arnold, I. Erb, M. Pachkov, N. Molina, E. van Nimwegen, MotEvo: integrated Bayesian probabilistic methods for inferring regulatory sites and motifs on multiple alignments of DNA sequences. *Bioinformatics* **28**, 487-494 (2012).
16. P. J. Balwierz *et al.*, Methods for analyzing deep sequencing expression data: constructing the human and mouse promoterome with deepCAGE data. *Genome Biol* **10**, R79 (2009).
17. M. Pachkov, P. J. Balwierz, P. Arnold, E. Ozonov, E. van Nimwegen, SwissRegulon, a database of genome-wide annotations of regulatory sites: recent updates. *Nucleic Acids Res* **41**, D214-D220 (2013).
18. Y. Zhang *et al.*, Model-based Analysis of ChIP-Seq (MACS). *Genome Biol* **9**, R137 (2008).
19. G. Yu, L.-G. Wang, Q.-Y. He, ChIPseeker: an R/Bioconductor package for ChIP peak annotation, comparison and visualization. *Bioinformatics* **31**, 2382-2383 (2015).
20. T. Hubbard *et al.*, The Ensembl genome database project. *Nucleic Acids Res* **30**, 38-41 (2002).
21. Y. Zhang, E. V. Laz, D. J. Waxman, Dynamic, Sex-Differential STAT5 and BCL6 Binding to Sex-Biased, Growth Hormone-Regulated Genes in Adult Mouse Liver. *Mol Cell Biol* **32**, 880-896 (2012).
22. B. D. Weger *et al.*, The Mouse Microbiome Is Required for Sex-Specific Diurnal Rhythms of Gene Expression and Metabolism. *Cell Metab* **29**, 362-382.e368 (2019).
23. P. J. Balwierz *et al.*, ISMARA: automated modeling of genomic signals as a democracy of regulatory motifs. *Genome Res* **24**, 869-884 (2014).

24. E. A. Niskanen, J. J. Palvimo, M. Malinen, P. Sipilä, ChIP-seq analysis of androgen receptor binding in epididymis of ArKI mice. *Gene Expression Omnibus (GEO)*, https://www.ncbi.nlm.nih.gov/geo/query/acc.cgi?acc=GSE121151 (2018).
25. J. Gertz, R. M. Myers, Distinct properties of cell type-specific and shared transcription factor binding sites. *Gene Expression Omnibus (GEO)*, https://www.ncbi.nlm.nih.gov/geo/query/acc.cgi?acc=GSE49993 (2013).
26. S. C. Hewitt *et al.*, A distal super enhancer mediates estrogen-dependent mouse uterine–specific gene transcription of Insulin-like growth factor 1 (Igf1). *Gene Expression Omnibus (GEO)*, https://www.ncbi.nlm.nih.gov/geo/query/acc.cgi?acc=GSE125972 (2019).
27. K. Mousavi *et al.*, eRNAs Promote Transcription by Establishing Chromatin Accessibility at Defined Genomic Loci. *Gene Expression Omnibus (GEO)*, https://www.ncbi.nlm.nih.gov/geo/query/acc.cgi?acc=GSE49313 (2013).